Journal of Operation and Automation in Power Engineering
Vol. 1, No. 2, Summer & Fall 2013, Pages: 110-123
http://journals.uma.ac.ir/joape

A Multi-Objective HBMO-Based New FC-MCR Compensator for Damping of Power System Oscillations

R. Ghanizadeh [1*], A. Jahandideh Shendi [2], M. Ebadian [3], M. Golkar [4], A. Ajami[5]
[1,3] Department of Electrical Engineering, University of Birjand, Birjand, Iran
[2] Department of Electrical Engineering, Islamic Azad University, Ahar Branch, Ahar, Iran
[4] Department of Electrical Engineering, K. N. Toosi University of Technology, Tehran, Iran
[5] Department of Electrical Engineering, Azarbaijan Shahid Madani University, Tabriz, Iran

ABSTRACT
In this paper, a novel compensator based on Magnetically Controlled Reactor with Fixed Capacitor banks (FC-MCR) is introduced and then power system stability in presence of this compensator is studied using an intelligent control method. The problem of robust FC-MCR-based damping controller design is formulated as a multi-objective optimization problem. The multi-objective problem is concocted to optimize a composite set of two eigenvalue-based objective functions comprising the desired damping factor, and the desired damping ratio of the lightly damped and undamped electromechanical modes. The controller is automatically tuned by optimization of an eigenvalue-based multi-objective function using Honey Bee Mating Optimization (HBMO) to simultaneously shift the lightly damped and undamped electromechanical modes to a prescribed zone in the s-plane so that the relative stability is guaranteed and the time domain specifications concurrently secured. The effectiveness of the proposed controller in damping low frequency oscillations under different operating conditions is demonstrated through eigenvalue analysis and nonlinear time simulation studies. The results show that the tuned HBMO-based FC-MCR controller which is designed by using the proposed multi-objective function has an outstanding capability in damping power system low frequency oscillations and significantly improves the power systems dynamic stability.

KEYWORDS: Magnetically Controlled Reactor with Fixed Capacitor Banks, Power System Dynamic Stability, Honey Bee Mating Optimization, Multi-objective Optimization.

1. INTRODUCTION

The main priorities in a power system operation are its security and stability, so a control system should maintain its frequency and voltage at a fixed level, against any kind of disturbance such as a sudden increase in the load, a generator being out of circuit, or failure of a transmission line because of factors such as human faults, technical defects of equipments, natural disasters, etc. Due to the new legislation of electricity market, this situation creates doubled stress for beneficiaries [1-2]. Low frequency oscillations within the range of 0.2 up to 3 Hz are created as large power systems are developed and connected to each other. These oscillations continue to exist in the system for a long time and if not well-damped, the amplitudes of these oscillations increase and bring about isolation and instability of the system [3-5]. Using a Power System Stabilizer (PSS) is technically and economically appropriate for damping oscillations and increasing the stability of power system. Therefore, various methods have been proposed for designing these stabilizers [6-8]. However, these stabilizers cause the power factor to

Recived: 28 Jan. 2013 Revised: 1 Apr. 2013
Accepted: 16 Apr. 2013
Corresponding author :
R. Ghanizadeh (E-mail: r_ghanizadeh@Birjand.ac.ir)

become leading and therefore, they have a major disadvantage which leads to loss of stability caused by large disturbances, particularly a three phase fault at the terminals of generator [9]. In recent years, using Flexible Alternating Current Transmission Systems (FACTS) has been proposed as one of the effective methods for improving system controllability and limitations of power transfer. By modeling bus voltage and phase shift between buses and reactance of transmission line, FACTS controllers can cause increment in power transfer in the steady state. These controllers are added to a power system for controlling normal steady state, but because of their rapid response, they can also be used for improving power system stability through damping the low frequency oscillation [1-6,10].

Static Var compensator (SVC) is a member of the FACTS devices family which is connected in parallel to the system.These compensators have faster response and better stability control than other compensators [11-13]. In spite of their advantages, these compensators also have some disadvantages including high THD and high maintenance costs [14-16]. Also, these compensators need a step-down transformer to make network voltage less than 35 kV and at the same time they need to use lots of power electronic elements both in series and parallel which increases loss and the cost of these compensators [17].

MCRs are powerful low-inertia inductors in which reactive power consumption can be regulated from 0.01 to 1.0 times the rated power with short term regulation (up to 1 min) up to 2.0 times the rated power. Because of this very wide range of control, MCRs reduce idle-mode power losses significantly. They also increase operational reliability of electrical grids and optimize power line operating conditions. MCRs increase power quality through automatic voltage regulation, reducing fluctuation, smoothing reactive power surges, damping voltage oscillations, increasing power stability limits and permitting higher voltage transmissions [17-19].

The MCR is controlled by changing magnetic permeability of the core. Magnetization of the steel is controlled by a DC current in control windings of the reactor, thus achieving magnetic biasing of the steel. MCR is based on two basic principles:

(1) The first principle of the MCR is the generation and control of the direct component of the magnetic flux in the MCR's two cores by periodic shorting of some of reactor winding turns by the use of semiconductor switches [18].
(2) The second principle of the MCR is profound magnetic saturation of the two cores under rated conditions, when the saturation magnetization generated by about half or more of the grid frequency period [14].

In this paper, the modified linearized Phillips-Heffron model is utilized to theoretically analyse a Single-Machine Infinite-Bus (SMIB) installed with an FC-MCR. Then, the results of this analysis is used for assessing the potential of an FC-MCR supplementary controller to improve the dynamic stability of a power system. The issue of designing a robust FC-MCR-based controller is considered and formulated as an optimization problem with aneigenvalue-based multi-objective function consisting of the damping ratios of the undamped electromechanical modes. Next, considering its high capability to find the most optimistic results, the HBMO is used to solve this optimization problem. A wide range of operating conditions are considered in the design process of the proposed damping controller in order to guarantee its robustness. The effectiveness of the proposed controller is demonstrated through eigenvalue analysis, controllability measure, nonlinear time-domain simulation. Results show that the proposed multi-objective function-based tuned damping controller achieves a good robust performance for a wide range of operating conditions and is superior to both controllers designed by using the single objective functions.

The rest of this paper is organized as follows: in Section 2, the HBMO is introduced. Section 3, fully describes the MCR theory. Nonlinear model of a SMIB system in presence of FC-MCR is presented and equations are thoroughly extracted in Section 4. In Section 5 robust controller design using multi-objective HBMO algorithm is presented. Finally, the robustness of the controller, eigenvalue analysis and nonlinear simulation of different modes of the system are presented. The last Section concludes the paper.

2. HONEY BEE MATING OPTIMIZATION

Bees are social insects that can only survive inside their colony. A bee activity shows various features such as group work and communication. In the bees social life usually there is a queen which lays eggs and has a longer life expectancy than other bees and usually, depending on the season, has about 60000 or more workers. Its life expectancy is about 5 or 6 years whereas the other bees especially the workers have a life expectancy that hardly reaches one year. Males or drones die after mating [20-21].

Insemination ends by the gradual death of drone bees. Each drone can take part in mating process just for one time, whereas queen can take part for several times. These features have made the mating process of bees more interesting than those of other insects. Mathematical description of the bee colony optimization is as follows:

A drone bee probabalistically mates a queen with the following probabilistic function:

$$\text{prob}(D,Q) = \exp(\frac{-\Delta(f)}{s(t)}) \quad (1)$$

where *prob(D,Q)* is the probability of adding the sperm of the drone bee *D*, into the womb of the queen *Q* (probability of successful mating). *Δ(f)* is the difference between fitness functions of the queen and the drone, and *S(t)* is the speed of queen at *t*. After each transfer in space, the speed and energy of queen is reduced according to the following equation:

$$s(t+1) = \alpha \times s(t) \quad (2)$$

$$s(t+1) = \alpha \times s(t) \quad (3)$$

In (2) and (3) α is a factor which varies between zero and one (for reducing queen speed) and γ is a coefficient in [0,1] which represents the amount of reduced energy after each mating process.

First, the queen speed is generated randomly. At the beginning of during-flight mating, males chosen by queen are generated randomly in (1). If mating is successful, the male's sperm will be stored in queen womb. By combining the queen and males genotypes a new baby is formed which can be grown by workers. One of the major differences between HBMO and old evolutionary algorithms is that the sperm storage takes place in queen womb because the queen uses it to produce a new solution for a baby with the highest level of capability. The following steps are considered for implementing HBMO algorithm:

- Defining input data.
- Generating initial population.
- Calculating the objective function.
- Classifying initial population according to the objective function values.
- Choosing the queen; the bee that has greater fitness value than others is chosen as the queen.
- Randomly generating the queen speed.
- Choosing initial population of male bees.
- generating the sperm womb of queen in flight mating.
- Egg-laying process of bees.
- Feeding the chosen babies and the queen with a jelly material by worker bees.
- Calculating the value of objective function for the created set of solutions.
- Checking the stopping criterion of the algorithm or the number of iterations.

At the end of the algorithm, if the stopping criterion is satisfied, the queen will be selected as the final solution otherwise, it returns to the third step and all the previous steps are repeated

till the stopping criterion is met. The computational flowchart of HBMO is shown in detail in Fig. 1.

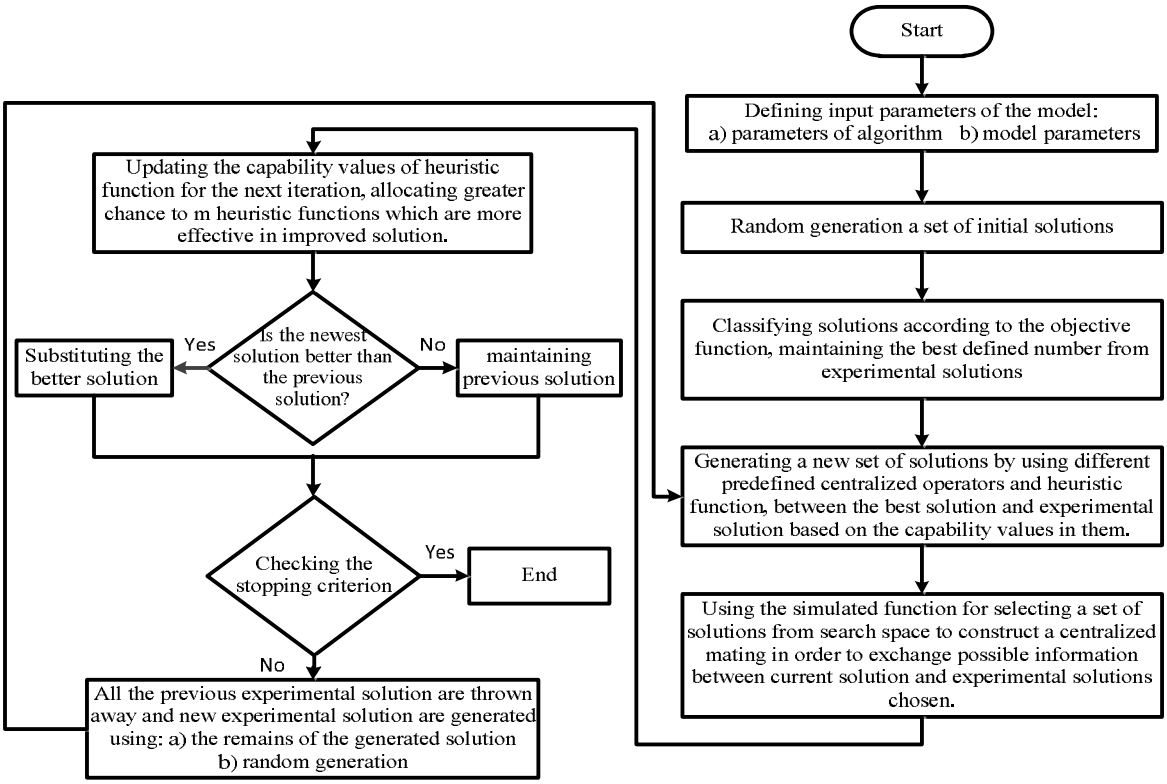

Fig. 1. The flowchart of HBMO algorithm.

3. THEORY OF MCR

3.1. MCR

The elementary MCR is shown in Fig. 2. The W_1 windings are placed in an AC circuit having an alternating current (i) and, while controlled by the W_2 windings which are joined to a DC source. If $\varphi = \varphi_m sin(wt)$ and $\varphi=f(HL)$, then for each value of W_2 with given curve [14], appropriate values of (HL) are found and a curve is built [14,18].

If the DC voltage in the W_2 windings is zero, then the current in windings of W_2 will also be zero. In this case, the current in windings of W_2 will produce sinusoidal flux, and the reactor current will be sinusoidal. Figure 3 (a) shows the magnetic flux and current when $I = 0$. If the DC voltage in windings of W_2 is not zero, then the current in windings of W_2 will not be zero either. In this case, the DC voltage produces constant flux (φ_0), and the total flux will be $\varphi = \varphi_m sin(wt)+\varphi_0$. Figure 3 (b) shows the magnetic flux and current when $I \neq 0$. Note that the current i does not contain a constant component, since there isn't any DC source in the circuit of W_1 windings.

The line A_1–A_2 in Fig. 3 (b) will be a zero line for curve $iw_1=f(wt)$. The currentin windings of W_2 changes around this straight line. Thus, the average current for the period which starts at $wt=0$ and ends at $wt=2\pi$ is equal to zero.

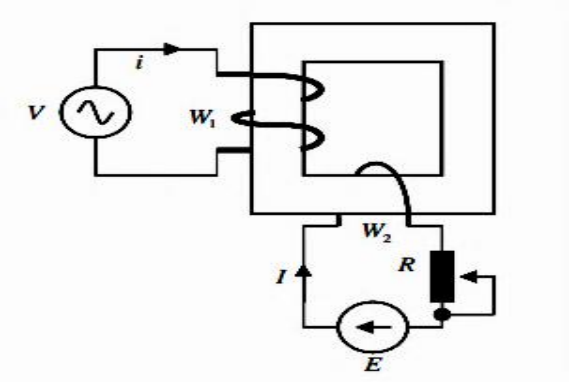

Fig. 2. The elementary controlled inductance

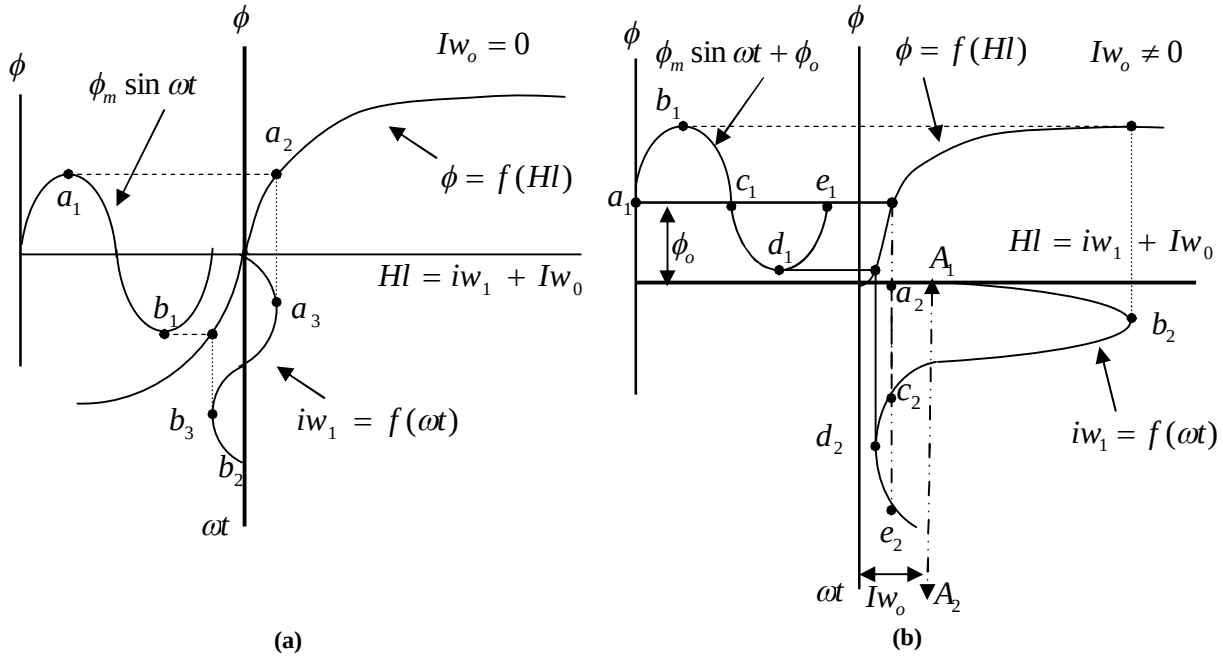

Fig. 3. Magnetic flux and current when: (a) $I = 0$ and (b) $I \neq 0$

3.2. Basic electric circuits of MCR

The basic electrical circuit of MCR is shown in Fig. 4 (a) [14-19], which is the basic idealized circuit for connecting windings of the two cores, in which the single-phase coincides with one of the widespread circuits of the magnetic amplifiers (Fig. 4 (a)).

There are two closed magnetic circuits, each of which is covered with half of CO winding and half of OY winding. The parts of the OY windings are connected consistently, and compared to the direction of current in CO windings, one has the same direction and the other one has the opposite direction (Fig. 4 (a)). Figure 4 (b) shows current in the CO windings at the voltage source (E) in OY windings. Under normal conditions ($E = 0$), the MCR is not saturated. When the voltage E starts to increase, the current of the MCR (i) in the windings of W_1 (Fig. 2) increases from zero to maximum, and the reactive power consumed in the reactor also increases. The current is essentially reactive and sinusoidal.

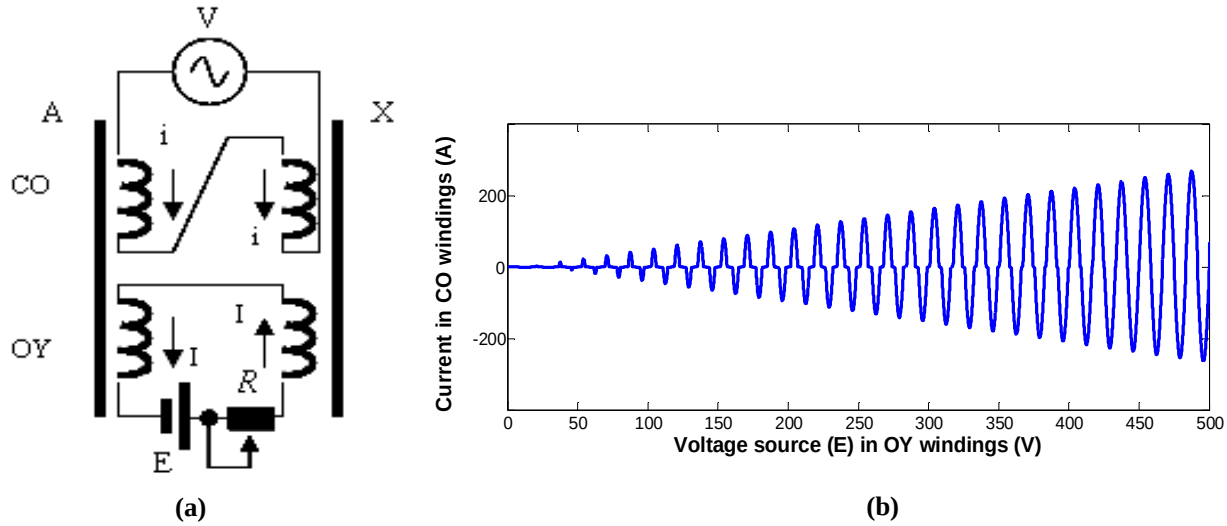

Fig. 4. (a) The basic electrical circuits of MCR. (b) current in CO windings at the voltage source E in OY windings.

4. DESCRIPTION OF CASE STUDY SYSTEM

Figure 5 shows a SMIB power system equipped with an FC-MCR. The synchronous generator is delivering power to the infinite-bus through a double circuit transmission line and an FC-MCR. The parameters of the test power system are given in the Appendix.

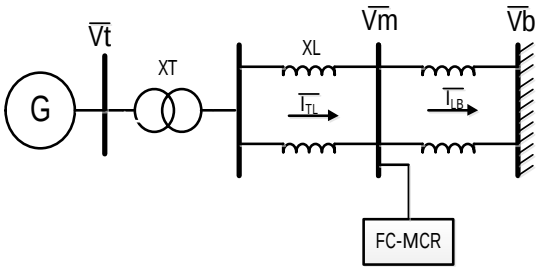

Fig. 5. SMIB power system equipped with FC-MCR

4.1. Power system nonlinear model with FC-MCR

Single-line schematic diagram of an FC-MCR compensator is shown in Fig. 6. The FC-MCR consists of (1) an MCR reactor, (2) a capacitor bank, (3) three-phase transformers with built-in thyristor converters for supplying the DC voltage, (4) control, safety, and automation systems for FC-MCR, (5) a voltage transformer and (6) a current transformer.

Fig. 6. Single-line circuit of FC-MCR compensator

Thiscompensator is investigated in two cases. In the first case, if the DC voltage applied to the FC-MCR is zero, no constant flux is added to the main flux and consequently the current of FC-MCR will be zero. Fig. 7 shows the flux and current curves of FC-MCR when the DC voltage is zero.

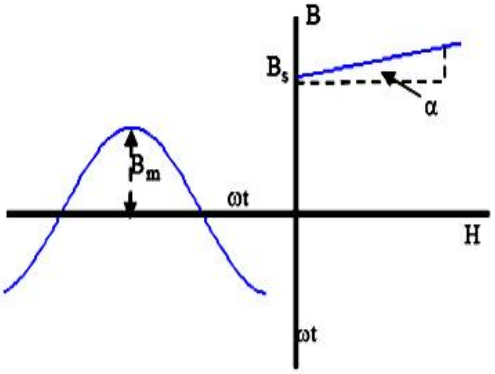

Fig. 7. Flux and current curves of the reactor when DC voltage is zero.

According to Fig. 7 it can be concluded that:

If $\varphi = 180, \sigma = 2(\pi - \varphi) \quad 0 \Rightarrow I_{reactor} = 0.$

In the second case, the DC voltage applied to the FC-MCR is not zero. This voltage generates a constant flux. Consequently, this flux is added to the main flux and as a result of intersection with magnetic saturation curve it generates the current of compensator. Figure 8 shows the flux and current curves of FC-MCR compensator when the DC voltage is not zero.

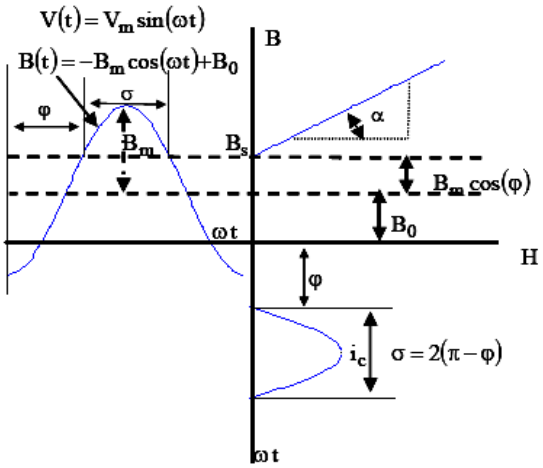

Fig. 8. Flux and current curves of the reactor when DC voltage is not zero.

According to Fig. 8, the value of magnetic flux density can be represented by:

$$B(t) = B_m \cos(\omega t) + B_0 \qquad (4)$$

The relationship between magnetic flux density (*B*) and magnetic field strength is indicated in Fig. 8. This figure reveals that for the positive half-wave,the magnetic field strength can be represented by the following equation:

$$H=\begin{cases} H_m(\cos(\varphi)-\cos(\omega t) & \varphi<\omega t<2\pi-\varphi \\ 0 & 2\pi-\varphi<\omega t<\varphi+\pi \end{cases} \quad (5)$$

where

$$H_m = B_m \cot(\alpha) = B_m \frac{1}{\tan(\alpha)} = \frac{\phi_m}{s}\cot(\alpha) = \frac{V_m}{s.\omega}\cot(\alpha) \quad (6)$$

According to (5) and (6), the current equation of FC-MCR can be obtained as:

$$I=\begin{cases} Im(\cos(\varphi)-\cos(\omega t) & \varphi<\omega t<2\pi-\varphi \\ 0 & 2\pi-\varphi<\omega t<\varphi+\pi \end{cases} \quad (7)$$

where,

$$I_m = H_m l \quad B_m l \cot(\alpha)$$
$$\frac{\phi_m}{s} l\cot(\alpha) = \frac{V_m.l}{s.\omega}\cot(\alpha) \quad (8)$$

In the above equations, α is the angle that is effective in the MCR current and is dependent on the core characteristic, and *S* is the cross-section area of the core.

The fundamental harmonic of FC-MCR current can be obtained by using Fourier analysis.

$$I = \frac{V.l}{\pi\omega s}\tan(\alpha)(2(\pi-\varphi)-\sin(2(\pi-\varphi)) \quad (9)$$

where, φ is the angle due to DC voltage.

$$I = B_c(\alpha)\cdot V \quad (10)$$

Thus:

$$B_c(\varphi) = \frac{1}{X_C} - \frac{1}{\pi X_L}(2(\pi-\varphi)-\sin(2(\pi-\varphi)) \quad (11)$$

In (11), $B_C(\varphi)$ is the adjustable susceptance in fundamental frequency and it is controlled by the angle generated by DC voltage.

Considering the investigated cases, FC-MCR compensator can be modeled by a first order dynamic equation with an acceptable precision. Figure 9 shows the structure of the FC-MCR-based damping controller. This controller may be considered as a lead-lag compensator. However, an electrical torque in phase with the speed deviation is to be produced to improve the damping of power system oscillations. It consists of a gain block, a signal-washout block, and a lead-lag compensator. The parameters of the damping controller are obtained using the HBMO technique.

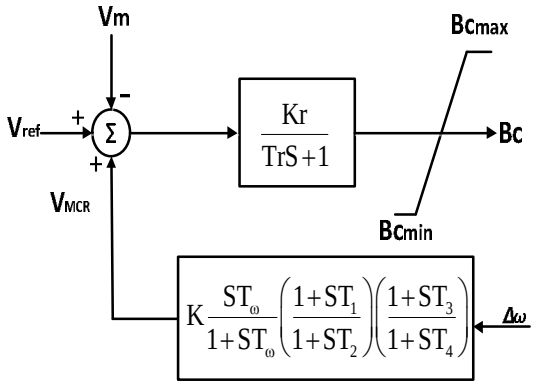

Fig. 9. Control block diagram of FC-MCR

According to Fig. 9, the following equation could be written:

$$\frac{K_r}{T_r S+1}(V_{ref}-V_m+U_{MCR}) = B_C \quad (12)$$

Equation (12) can be written as follows:

$$\dot{B}_C = -\frac{1}{T_r}B_C + \frac{K_r}{T_r}(V_{ref}-V_m+U_{MCR}) \quad (13)$$

where, B_C is susceptance, K_r and T_r are the gain and time constants considered for thyristors firing angles.

The nonlinear model of SMIB system shown in Fig. 5 is described by [1]:

$$\dot{\delta} = \omega_o(\omega-1) \quad (14)$$

$$\dot{\omega} = \frac{1}{M}(P_m - P_e - D\Delta\omega) \quad (15)$$

$$\dot{E}'_q = \frac{1}{T'_{do}}(E_{fd}-E_q) \quad (16)$$

$$\dot{E}_{fd} = -\frac{1}{T_A}E_{fd} + \frac{K_A}{T_A}(V_{ref}-V_t) \quad (17)$$

where

$$P_e = E'_q I_q + (X_q - X'_d)I_d I_q$$
$$E_q = E'_q + (x_d - x'_d).I_d$$
$$V_t = \sqrt{(X_q I_q)^2 + (E'q - X'_d I_q)^2}$$

$$V_m = \sqrt{(E'q - (X'_d + X_{L1} + X_T)I_d)^2 + ((X_q + X_{L1} + X_T)I_q)^2}$$

$$I_d = \frac{E'q(1 - X_{L2}B_C)}{X_D} - \frac{V_b \cos(\delta)}{X_D},\ I_q = -\frac{V_b \sin(\delta)}{X_Q}$$

$$X_D = (X'_d + X_{L1} + X_T + X_{L2}) - (X'_d(X_{L1} + X_T) + (X_{L1} + X_T)X_{L2})$$

$$X_Q = -(X'_q + X_{L1} + X_T + X_{L2}) + (X'_q(X_{L1} + X_T) + (X_{L1} + X_T)X_{L2})$$

4.2. Power system linearized model

A linear dynamic model is obtained by linearizing the nonlinear model around an operating condition. The linearized model of power system as shown in Fig. 5, is given as follows:

$$\Delta\dot{\delta} = \omega_o.\Delta\omega \tag{18}$$

$$\Delta\dot{\omega} = \frac{1}{M}(\Delta T_m - K_1.\Delta\delta - K_2\Delta E'_q - K_3.\Delta B_C - k_d\Delta\omega) \tag{19}$$

$$\Delta\dot{E}'_q = \frac{1}{T'_{do}}(\Delta E_{fd} + K_4.\Delta\delta + K_5\Delta E'_q + K_6\Delta B_C) \tag{20}$$

$$\Delta\dot{E}_{fd} = -\frac{1}{T_A}\Delta E_{fd} + \frac{K_A}{T_A}(\Delta V_{ref} - K_7.\Delta\delta - K_8.\Delta E'_q - K_9.\Delta B_C) \tag{21}$$

$$\Delta\dot{B}_C = -\frac{1}{T_r}\Delta E_{fd} + \frac{K_r}{T_r}(-K_{10}.\Delta\delta - K_{11}.\Delta E'_q - K_{12}.\Delta B_C + \Delta\omega) \tag{22}$$

where, K_1, K_2, ..., K_{12} are linearization constants. System state space model is obtained as follows:

$$\dot{x} = Ax + Bu \tag{23}$$

where, x is the state vector and u is control vector, A and B are:

$$A = \begin{bmatrix} 0 & \omega_b & 0 & 0 & 0 \\ -\frac{K_1}{M} & -\frac{K_d}{M} & -\frac{K_2}{M} & 0 & -\frac{K_3}{M} \\ \frac{K_4}{T'_{do}} & 0 & -\frac{K_5}{T'_{do}} & -\frac{1}{T'_{do}} & -\frac{K_6}{T'_{do}} \\ -\frac{K_a K_7}{T_A} & 0 & -\frac{K_A K_8}{T_A} & -\frac{1}{T_A} & -\frac{K_A K_9}{T_A} \\ -\frac{K_r K_{10}}{T_r} & 0 & -\frac{K_r K_{11}}{T_r} & 0 & -\frac{1 + K_r K_{12}}{T_r} \end{bmatrix}$$

$$B = \begin{bmatrix} 0 & 0 & 0 \\ \frac{1}{M} & 0 & 0 \\ 0 & 0 & 0 \\ 0 & \frac{K_A}{T_A} & 0 \\ 0 & 0 & \frac{K_r}{T_r} \end{bmatrix}$$

The block diagram of the linearized dynamic model of the SMIB power system with FC-MCR is shown in Fig. 10.

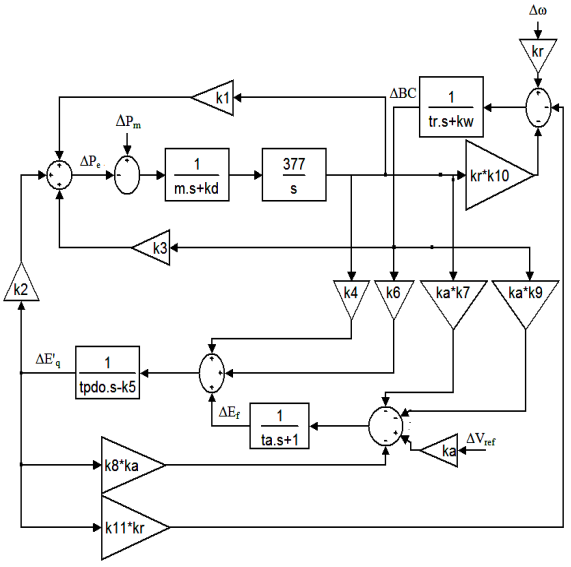

Fig. 10. Phillips-Heffron model of SMIB power system with FC-MCR

5. FC-MCR CONTROLLER DESIGN USING HBMO

In this proposed method, parameters of FC-MCR controller are optimally adjusted for dynamic stability of the entire system. Considering the fact that the selection of gains of output feedback for FC-MCR as a damping controller is a complicated optimization problem, thus to increase the system damping for electromechanical modes, a multi-objective function based on eigenvalues is considered which includes two separate objective functions that form a compound objective function with an appropriate weight ratio [3]. The HBMO algorithm is used to obtain optimum values for the objective function. The multi-objective function with an appropriate weight ratio is considered as following:

$$J_1 = \sum_{j=1}^{NP} \sum_{\sigma_i \geq \sigma_0} (\sigma_0 - \sigma_i)^2,$$
$$J_2 = \sum_{j=1}^{NP} \sum_{\xi_i \leq \xi_0} (\xi_0 - \xi_i)^2, \quad (24)$$
$$J = J_1 + aJ_2$$

where, $\sigma_{i,j}$ and $\zeta_{i,j}$ are real part and damping ratio of i^{th} eigenvalue in j^{th} operating point, respectively. The value of α is equal to 10 and *NP* is equal to the number of operating points in optimization problem. By considering J_1, the dominant eigenvalues are transferred to the left side of the line $s = \sigma_0$ in the S-plane according to Fig. 11 (a). This provides relative stability in the system. Similarly, if we consider objective function J_2, the maximum overshoot of eigenvalues becomes limited and eigenvalues are transmitted to the specified area which is shown in Fig. 11 (b). Multi-purpose objective function J transmits the eigenvalues of the system to the specified area shown in Fig. 11 (c).

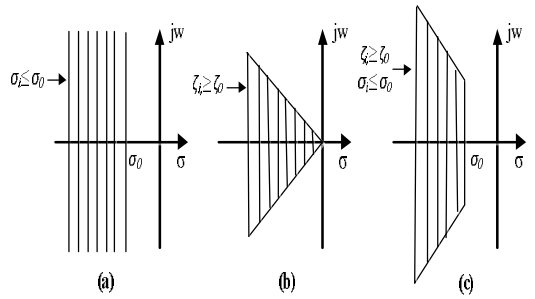

Fig. 11. Eigenvalue location for the objective function

The designing problem is formulated as a constrained optimization problem where the constraints are as follows:

$$K_{\min} \leq K \leq K_{\max}$$
$$T_{1\min} \leq T_1 \leq T_{1\max}$$
$$T_{2\min} \leq T_2 \leq T_{2\max} \quad (26)$$
$$T_{3\min} \leq T_3 \leq T_{3\max}$$
$$T_{4\min} \leq T_4 \leq T_{4\max}$$

The proposed method uses HBMO intelligent algorithm to solve the optimization problem to obtain an optimal set for controller parameters. The objective function given in (24) takes place in different performance conditions of system, the desired performance conditions are considered as in Table 1.

Table 1. Loading condition

Operating conditions	*P (pu)*	*Q (pu)*	X_L*(pu)*
Base case	0.8	0.2629	0.3
Case 1	0.8	0.2629	0.6
Case2	0.4	0.1314	0.3
Case 3	0.4	0.1314	0.6
Case 4	1.2	0.39	0.3
Case 5	1.2	0.39	0.6

In this work, the range of optimization parameters is selected to be [1-100] for *K*, also [0.01-1]is the selected range for parameters T_1, T_2, T_3 and T_4. For achieving a better performance of HBMO, the number of queens, drones, and workers, the size of womb and the maximum number of mating process are considered 1, 100, 1000, 50 and 30, respectively. The proposed optimization algorithms have been implemented several times, then a set of optimal values is selected. The final values of the optimized parameters with both single objective functions J_1, J_2 and the multi-objective function J are given in Table 2.

5. SIMULATION RESULTS

In order to demonstrate the effectiveness and robustness of the proposed controller, against severe turbulence and the damping of oscillations caused by it, power system using the proposed model, is simulated in MATLAB software.

Table 2. The optimal parameter settings of the proposed controllers based on the different objective function

Controller parametes	J_1	J_2	J
K	83.8019	74.22	90.2856
T_1	0.7008	0.9275	0.9698
T_2	0.4822	0.7604	0.6382
T_3	0.9978	0.8061	0.7624
T_4	0.0669	0.0114	0.4076

To make sure that the obtained results are reliable, this simulation is evaluated with eigenvalue analysis method and time domain nonlinear simulation, which is shown as follows.

5.1. Eigenvalue analysis

The electromechanical modes and the damping ratios obtained for all operating conditions both with and without proposed controllers in the system are given in Table 3. When FC-MCR is not installed, it could be seen that some of the modes are poorly damped and in some cases, they are unstable (highlighted in Table 3). It is also clear that the system damping with the proposed *J*-based tuned FC-MCR controller is significantly improved.

Table 3. Eigenvalues and damping ratios of electromechanical modes with and without controller

Operating conditions	Type of controller			
	Without controller (damping ratio)	J_1(damping ratio)	J_2 (damping ratio)	J (damping ratio)
Base case	-80.3027 **0.3072 ± 4.2420i, (-0.0722)** -7.1274, -4.379	-2.9283± 4.1753i, (0.5741) -7.304, -6.1269 -3.8572, -1.571 -1.05, -81.831	-1.8416± 4.394i, (0.3865) -9.73, -5.4797 -3.1912, -1.3421 -1.04, -83.1529	-2.9087 ± 6.4271i, (0.412) -1.6219 ± 1.8341i, (0.662) -5.9853, -1.3466 -1.18, -85.1572
Case 1	-83.3126 **0.548± 5.138i, (-0.106)** -6.1493 ± 0.4276i, (0.9975)	-6.1452 ± 3.193i, (0.8873) -3.938 ± 2.646i, (0.83) -3.217, -1.972 -1.08, -86.3265	-2.3775 ± 4.122i, (0.499) -6.6462 ± 2.5437i, (0.933) -13.26, -1.9532 -1.04, -83.186	-6.0921 ±8.2326i, (0.5948) -2.6142 ± 2.5381i, (0.717) -14.321, -1.9742 -1.05, -84.3192
Case 2	-86.042 **0.7049 ± 3.1710i, (-0.216)** -4.9072, -1.294	-0.8386 ± 2.9085i, (0.277) -7.5732, -2.745 -2.6552, -1.4461 -1.02, -87.973	-1.5175 ± 2.2171i, (0.564) -11.263, -3.8616 -1.541, -1.1943 -1.026, -86.393	-2.2972 ± 4.6514i,(0.469) -1.3954 ± 1.9535i, (0.581) -1.9413, -1.8319 -1.03, -88.214
Case 3	-80.1276 **0.3052 ± 4.372i, (-0.0696)** -7.164, -2.963	-2.9813± 4.7511i, (0.531) -7.341, -7.7268 -3.4872, -1.7157 -1.05, -81.8332	-1.8414± 4.395i, (0.3864) -9.493, -5.7963 -3.9536, -1.2341 -1.03, -83.7158	-2.9874 ± 6.473i, (0.4458) -1.2194 ± 1.4119i, (0.653) -5.8529, -1.4612 -1.02, -85.6738
Case 4	-83.1364 **0.5860± 5.1389i, (-0.1132)** -6.935 ± 0.4276i, (0.9981)	-4.1452 ± 4.983i, (0.6395) -2.862 ± 2.1452i, (0.8001) -5.218, -1.9487 -1.08, -86.8326	-2.3791 ± 4.2719i,(0.486) -5.4658 ± 1.762i,(0.9517) -13.46, -1.4953 -1.04, -83.49	-4.2138 ±8.3868i, (0.487) -2.8642 ± 1.438i, (0.893) -14.323, -1.9741 -1.05, -84.5371
Case 5	-86.942 **0.7649 ± 2.4710i, (-0.2957)** -4.1972, -1.473	-0.8438 ± 2.9985i, (0.270) -7.4537, -3.945 -1.6523, -1.3961 -1.02, -87.569	-1.3475 ± 2.1971i, (0.522) -11.206, -3.3624 -1.396, -1.9463 -1.031, -86.3912	-2.2971 ± 4.6517i, (0.442) -1.3957 ± 1.9535i, (0.581) -1.4043, -1.4315 -1.03, -88.0218

5.2. Nonlinear time-domain simulation

The single-machine infinite-bus system shown in Fig. 5 is considered for nonlinear simulation studies. A 6-cycle 3-phase fault at t = 1 s, on the infinite bus has occurred, in all of the loading conditions given in Table 1, to study the performance of the proposed controller. The performance of the controller when the multi-objective function is used in the design is compared to that of the controllers designed using the single objective functions J_1 and J_2. The speed deviation, electric power deviation, and susceptance deviation based on the controller in six different loading conditions are shown in Figs. 12, 13, 14, 15, 16 and 17 respectively. It can be seen that the HBMO-based FC-MCR controller tuned using the multi-objective function achieves good robust performance, provides superior damping in comparison with the other objective functions and enhance greatly the dynamic stability of power systems.

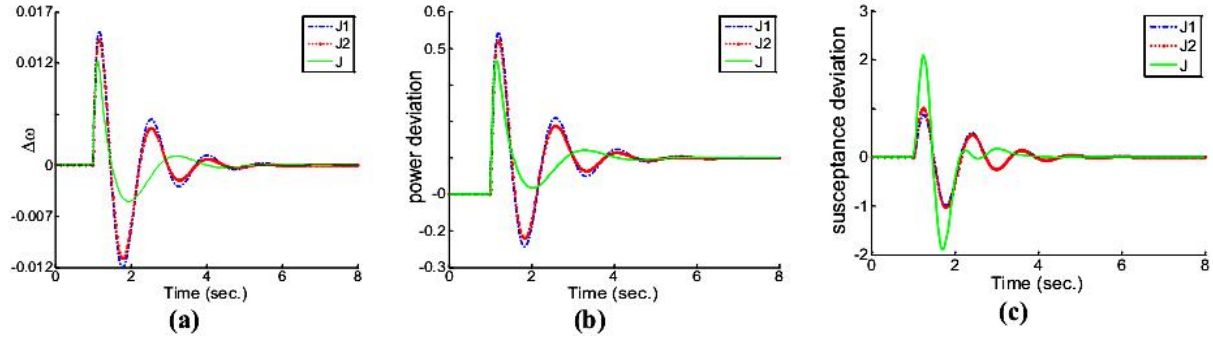

Fig. 12. Dynamic responses for (a) $\Delta\omega$ (b) ΔP (c) ΔB_C with controller at base case loading condition

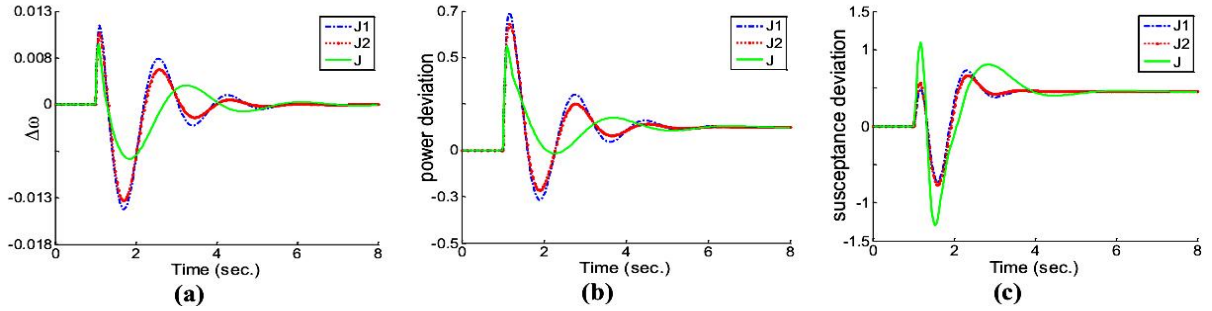

Fig. 13. Dynamic responses for (a) $\Delta\omega$ (b) ΔP (c) ΔB_C with controller at case 1 loading condition

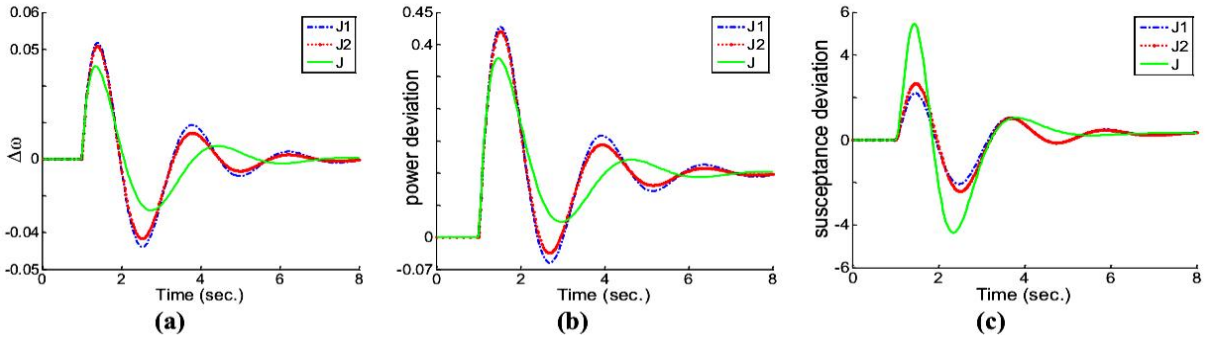

Fig. 14. Dynamic responses for (a) $\Delta\omega$ (b) ΔP (c) ΔB_C with controller at case 2 loading condition

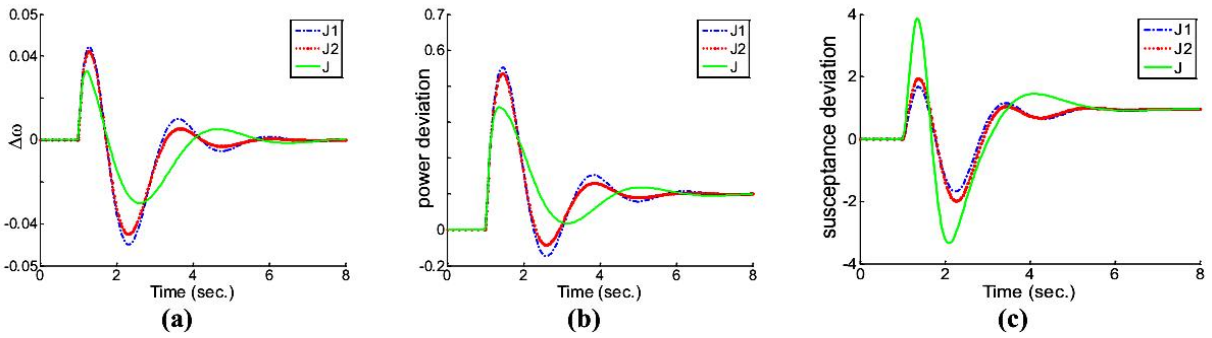

Fig. 15. Dynamic responses for (a) (a) $\Delta\omega$ (b) ΔP (c) ΔB_C with controller at case 3 loading condition**.**

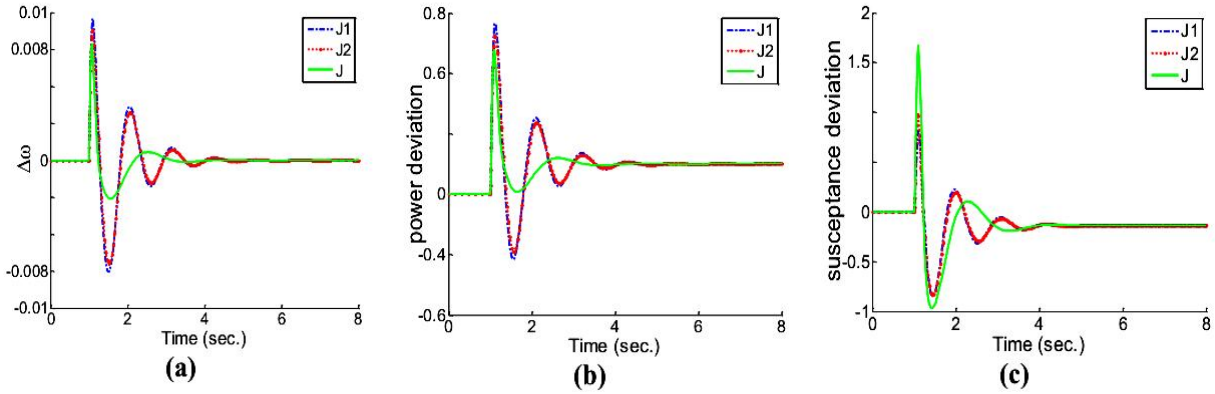

Fig. 16. Dynamic responses for (a) $\Delta\omega$ (b) ΔP (c) ΔB_C with controller at case 4 loading condition

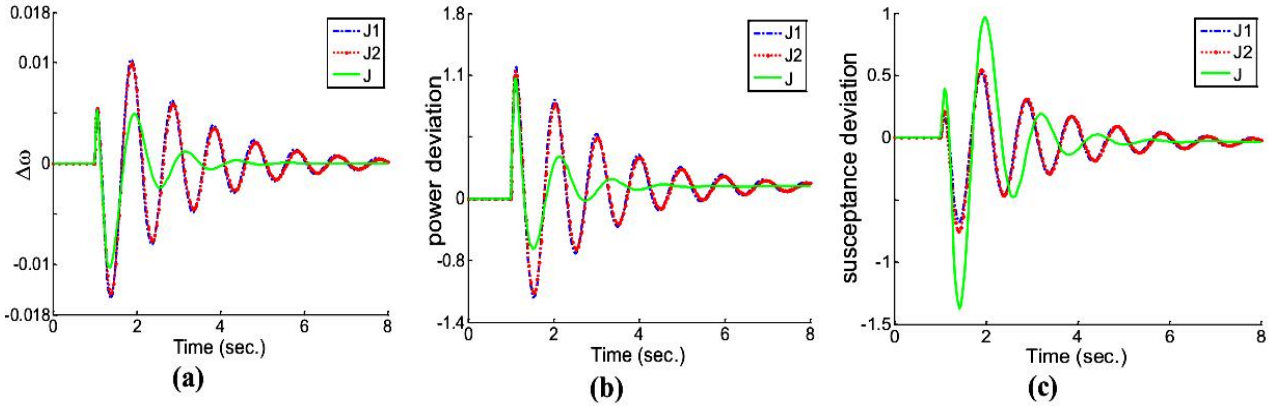

Fig. 17. Dynamic responses for (a) $\Delta\omega$ (b) ΔP (c) ΔB_C with controller at case 5 loading condition.

5. CONCLUSION

In this paper, state space model of a new FC-MCR compensator was extracted and transient stability performance improvement by using an FC-MCR controller investigated. The stabilizers were tuned to simultaneously shift the undamped electromechanical modes of the machine to a prescribed zone in the s-plane. A multi-objective problem was formulated to optimize a composite set of objective functions comprising the damping factor, and the damping ratios of the undamped electromechanical modes. The design problem of the controller was converted into an optimization problem which solved by HBMO technique with an eigenvalue-based multi-objective function. The effectiveness of the proposed FC-MCR controllers was demonstrated for improving transient stability performance of a power system by a weakly connected example power system subjected to different severe disturbances. The eigenvalue analysis and nonlinear time-domain simulation results show the effectiveness of the proposed controller using multi-objective function and their ability to provide good damping of low frequency oscillations.

APPENDIX

The test system parameters are:

Generator

M = 8 MJ/MVA, T'_{do}=5.044, X_d=1 pu, X_q=0.6 pu, X'_d=0.3 pu, D=4

Excitation system

K_A=80, T_A=0.05s

Transformers

X_T=0.1 pu, X_{SDT}=0.1 pu

Transmission line

X_L=0.6 pu

FC_MCR parameters

K_r=1, T_r=0.3, T_w=10.

REFERENCES

[1] A.T. Al-Awami, Y. L. Abdel-Magid and M. A. Abido, "A particle-swarm-based approach of power system stability enhancement with unified power flow controller," *International Journal of Electrical Power and Energy Systems*, vol. 29, no. 3, pp. 251–259, 2007.

[2] P. M. Anderson and A. A. Fouad, "Power System Control and Stability," *Ames, IA: Iowa State University* .Press ,1977.

[3] H. Shayeghi, H. A. Shayanfar, S. Jalilzadeh and A. Safari,"A PSO based unified power flow controller for damping of power system oscillations," *Energy Conversion and Management*, vol. 50, no.10, pp. 2583-2592, 2009.

[4] H. Shayeghi, H. A. Shayanfar, S. Jalilzadeh and A. Safari,"Design of output feedback UPFC controller for damping of electromechanical oscillations using PSO," *Energy Conversion and Management*, vol. 50, no.10, pp. 2554-2561, 2009.

[5] A. Ajami and M. Armaghan,"Application of multi-objective PSO algorithm for power system stability enhancement by means of SSSC," *International Journal of Computer and Electrical Engineering*, vol. 2, no. 5, pp. 1793-8163, 2010.

[6] M.A. Abido, "Robust design of multimachine power system stabilizers using simulated annealing," *IEEE Transactions on Energy Conversion*, vol. 15, no. 3, pp. 297-304, 2000.

[7] L. Chun, R. Yokoyama, K. Koyanagi and Y.L. Kwang, "PSS design for damping of inter-area power oscillations by coherency-based equivalent model," *International Journal of Electrical Power and Energy Systems*, vol. 26, no. 7, pp. 535-544, 2004.

[8] P. Kundur, M. Klein, G.J. Rogers and M.S. Zywno, "Application of power system stabilizers for enhancement of overall system stability", *IEEE Transactions on Power Systems*, vol. 4, no. 2, pp. 614-626, 1989.

[9] A.J.F. Keri, X. Lombard and A.A. Edris, "Unified power flow controller: modeling and analysis," *IEEE Transactions on Power Systems*, vol. 14, no. 2, pp. 648-654, 1999.

[10] M.R. Banaei and A. Kami, "Interline power flow controller (IPFC) based damping recurrent neural network controllers for enhancing stability," *Energy Conversion and Management*, vol. 52, no.7, pp. 2629-2636, 2011.

[11] D. Lijie, L. Yang, M. Yiqun, "Comparison of high capacity SVC and STATCOM in real power grid, " *Proceedings of the International Conference on Intelligent Computation Technology and Automation*, pp. 993- 997, 2010.

[12] S.M. Abd-Elazim and E.S. Ali, "Bacteria foraging optimization algorithm based SVC damping controller design for power system stability enhancement," *International Journal of Electrical Power and Energy Systems*, vol. 43, no.1, pp. 933-940, 2012.

[13] S.M. Abd-Elazim and E. S. Ali, "Coordinated design of PSSs and SVC via bacteria foraging optimization algorithm in a multimachine power system," *International Journal of Electrical Power and Energy Systems*, vol. 41, no.1, pp. 44-53, 2012.

[14] R.R. Karymov and M. Ebadian, "Comparison of magnetically controlled reactor (MCR) and thyristor controlled reactor (TCR) from harmonics point of view," *International Journal of Electrical Power and Energy Systems*, vol. 29, no. 3, pp.191-198, 2007.

[15] R. Ghanizadeh, M. Delbari and M. Ebadian, "Matimaticall modeling and harmonics optimization of a multi-level magnetically controlled reactor with harmony search algorithm," *International Review on Modelling and Simulations*, vol. 5, no. 4, pp. 1858-1866, 2012.

[16] M. Ebadian and A.A. Samadi, "High order harmonics reduction in magnetically controlled reactor (MCR)," *International Journal of Electrical Engineering*, vol. 6, no. 3, pp. 519-525, 2009.

[17] R. Ghanizadeh, M. Ebadian and M.A. Golkar, "Performance comparison of a new compensator based on magnetically controlled reactor and static var compensator (SVC)," *International Review on Modelling and Simulations*, vol. 5, no. 4, pp.1664-1671, 2012.

[18] M. Ebadin and F. Dstyar, "Performance comparison of transient behaviors of magnetically and thyristor-controlled reactors," *Electric Power Components and System*, vol.

38, no. 1, pp.85-99, 2009.

[19] M. Ebadian, R. Ghanizadeh and M. Delbari, "Assignment of magnetically controlled reactor (MCR) parameters considering minimization of power losses," *International Review on Modelling and Simulations*, vol. 5, no. 1, pp. 517-524, 2012.

[20] A. Afshar, B. Haddad, M.A. Marino, Adams B.J., "Honey bee mating optimization (HBMO) algorithm for optimal reservoir operation," *Journal of franklin Institute*, vol. 344, no. 5, pp. 452- 462, 2007.

[21] T. Niknam, H.D. Mojarrad, H. Zeinoddini, B.B. Firouzi, "A new honey bee mating optimization algorithm for non-smooth economic dispatch," *Energy*, vol. 36, no. 2, pp. 896-908, 2011.